Heliyon 10 (2024) e23145

Contents lists available at ScienceDirect

Heliyon

journal homepage: www.cell.com/heliyon

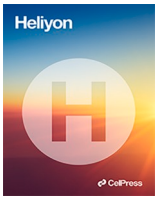

Optimization and evaluation of the distribution of Fischer-Tropsch products over a cobalt-based catalyst utilising design expert software

Roick Chikati [a], Tawanda A. Mpandanyama [a], Diankanua Nkazi [a], Phathutshedzo Khangale [b], Joshua Gorimbo [c,*]

[a] Department of Chemical and Metallurgical Engineering, University of the Witwatersrand, Johannesburg, South Africa
[b] Department of Chemical Engineering, University of Johannesburg, Doornfontein, 2028, Johannesburg, South Africa
[c] Institute for Catalysis and Energy Solution (ICES), College of Science, Engineering and Technology, University of South Africa (UNISA), Private Bag X6, Florida, 1710, Johannesburg, South Africa

ARTICLE INFO

Keywords:
Fischer-Tropsch synthesis (FTS)
Clinoptilolite
Response surface methodology (RSM)
Design of experiments (DOE)

ABSTRACT

Modelling biomass to liquid via the Fischer-Tropsch synthesis (FTS) system allows researchers to investigate the most efficient parameters while running the system under optimal conditions. As part of the design of experiments (DOE) procedure, a special data simulation method based on response surface methodology (RSM) is utilized to thoroughly analyse the impact of operating circumstances. The objective of this study was to examine the factors that affect the production of C_1, C_2–C_4, and C_{5+} in FTS process, and then optimize the critical factors utilising factorial design and response surface techniques. The parameters evaluated were reaction temperature, reaction pressure and the crystallite size of cobalt. The effects of these factors and their potential for synergy were explored simultaneously using multivariate DOE, with the yield of different hydrocarbon composition selectivity's as the measured responses. In the concept generation phase, optimization was based on the literature consulted, which proved to be an effective method for determining the optimization parameters. The detailed conceptual design included the generation of models using statistical methods and response surface models. Finally, the optimized design was validated using catalysts and parameters obtained during the optimization process, and this were compared to the output recorded in the theoretical modelling. The optimized parameters resulted in performance consistency, with the theoretical model for each group of hydrocarbons being validated by actual experiments. The established models were seen to characterize hydrocarbon distributions accurately and repeatedly over a wide range of reaction conditions (200–270 °C, 5–20 Bar, and 3–26 nm) using a cobalt-based catalyst. According to the detailed quantitative models developed, for higher C_{5+} production, 220 °C, 10 bar_g and 11 nm (cobalt crystallite) benchmark parameters were set to produce 19.3 % C_1, 11.4 % C_2–C_4 and 69 % C_{5+} selectivity's. Comparative analysis showed a 1.9 %, 3.9 % and 0.3 % percentage difference between the theoretical output and the actual output of C_1, C_2–C_4 and C_{5+}, respectively.

* Corresponding author.
E-mail address: gorimj@unisa.ac.za (J. Gorimbo).

https://doi.org/10.1016/j.heliyon.2023.e23145
Received 10 May 2023; Received in revised form 10 November 2023; Accepted 27 November 2023
Available online 14 December 2023

1. Introduction

Fischer-Tropsch synthesis (FTS) is receiving attention as a potentially game-changing method to cut pollution and make the transition to a more sustainable form of energy [1,2]. FTS transforms carbon dioxide (CO_2) and hydrogen gas (H_2) into useful hydrocarbons with reduced emissions of burn-off pollutants. This transformation normally takes place at a low pressure and a low temperature, and the stoichiometric ratio of H_2 to CO is 2:1 [3]. In addition, the pressure and temperature levels used during this operation are normally quite moderate [4–6]. The utilization of metal catalysts and a variety of supports has been the focus of most of the research on CO and H_2 conversion, which ultimately results in the production of lightweight and heavyweight hydrocarbons. However, it is still difficult to exercise control over the production of required compounds.

Cobalt and iron were considered as the first active catalysts used in the production of hydrocarbons via FTS [7–10]. Cobalt catalysts are costly, although relatively cheaper than ruthenium, because they show functionality at lower synthesis pressure and temperatures levels, which means that the higher catalyst cost is counter-balanced by the reduced operating cost [11]. They are also less vulnerable to deactivation [11]. Moreover, cobalt-based catalysts show improved conversion productivity compared to their iron counterparts [12].

Multiple factors affect the selectivity of Fischer-Tropsch (FT) catalysts, including reaction temperature, reaction pressure, feed composition, catalyst crystallite size [13], residence time [9,14], flow rate [15] and reactor type [9]. Slight changes in parameters can significantly change the selectivity of FT catalysts. Therefore, these variables should be monitored. Cobalt-based catalysts are preferred to produce long chain hydrocarbons in low-temperature FT reactions, because of the low water gas shift activity. In addition, cobalt selectively forms linear paraffins [4,16]. Cobalt is a relatively expensive metal, so it is important to maximize the available metallic surface area of cobalt in the catalyst while minimizing the amount of cobalt used. This is achieved by dispersing cobalt on high surface area supports. While dispersion is important, operating conditions also have an impact on catalyst selectivity, and it is critical to identify methods of monitoring the catalytic activity of the catalyst.

One of the noteworthy characteristics of Fischer-Tropsch Synthesis (FTS) is its operation under conditions of low pressure and temperature, combined with a stoichiometric ratio of hydrogen (H_2) to carbon monoxide (CO) at 2:1 [17,18]. These operational conditions not only enhance energy efficiency but also play a pivotal role in minimizing the environmental footprint. This underscores the paramount importance of optimizing the FTS process.

However, the complexity of FTS results in the generation of a wide array of products, necessitating the optimized selection of experimental conditions to achieve desired outcomes. In the context of this research the optimization technique of Response Surface Methodology (RSM) to systematically identify and refine the optimal process parameters, particularly concerning the catalyst will be used. RSM will offers a methodical approach to achieve a comprehensive understanding of the multifaceted interplay of variables and ultimately enhances the efficiency and effectiveness of FTS.

Response surface methodology (RSM) is a tool used for designing experiments that is oftenly used in the development and optimization of process and synthesis parameters [19]. The technique needs minimum experimentation and time and has proved to be more effective and more cost-effective than conventional methods used to design a synthesis and operation process. Furthermore, the use of Design Expert - a DOE approach - validates the efficiency. Manipulation of individual experimental conditions is traditionally studied using the one-factor-at-a-time (OFAT) approach. This format is time-consuming and tedious [20] compared to the DOE approach, which has the advantage of detecting interaction between the process factors.

The purpose of this study was to investigate the interactions between process factors during FT experiments. The investigation also aimed to determine the activity and selectivity of cobalt-based catalysts, with the focus being their role in hydrocarbon generation. The effect of crystallite size on clinoptilolite supports was also investigated. This was done to compare catalytic performances across a variety of operating conditions, the objective being to identify conditions that produce maximum C_{5+} and to identify how changing variables affect C_{5+} production.

2. Experimental

2.1. Catalyst preparation

2.1.1. Synthesis of 10 wt%cobalt on clinoptilolite (10 wt%Co/Clino for nomenclature)

Natural zeolite (clinoptilolite) samples obtained from Pratley Minerals in Krugersdorp, South Africa, were crushed using ring pulverisers. The powdered zeolite was then passed through a series of sieves with successively decreasing mesh sizes, the size ranges being −212 to +150 μm, then −150 to +106 μm, then −106 to +75 μm, then −75 to +53 μm, then −53 to +38 μm, then −38 to +25 μm, and lastly 25 μm. Only three of the seven clinoptilolite size classes (−75 to +53 μm, −53 to +38 μm, and −25 μm) were chosen for testing for use as a support in the synthesis of a cobalt catalyst. The basis for this decision was determined by preliminary characterization experiments, which also revealed substantial differences in activation energy levels and particle size. Additionally, the number of samples to be analysed was constrained by the equipment used, as the rig employed in this investigation only contained three reactors, which had to run simultaneously.

The correct amount of cobalt was deposited on each individual clinoptilolite support to produce 10 % wt Co/Clino. Sigma-Aldrich supplied the cobalt (II) nitrate hexahydrate required to synthesize the catalyst. A measure of 100 g of pure clinoptilolite (of various size classes) was placed in a beaker. Next, 54.82 g of cobalt (II) nitrate hexahydrate were weighed and diluted in 70 mL of ethanol (based on the pore volume of the clinoptilolite support). The solution was stirred with a magnetic stirrer for the allotted period (30 min). The solution was then added in drops to the clinoptilolite, which was agitated for an hour with a magnetic stirrer. It was then sonicated

ultrasonically for half-an-hour. The sample was allowed to air-dry at room temperature for 24 h before being heated to 110 °C for 6 h. The dried sample was calcined in air at 350 °C for 6 h.

2.2. Material characterization

2.2.1. X-ray diffraction

The powder x-ray diffraction (XRD) technique was carried out using a Rigaku Ultima IV X-ray diffractometer at a scanning speed of 0.5^o/min, from 10^o to 90^o 2-theta angle, to obtain the diffraction patterns of the sample. The voltage and current of the x-ray source were set to 40 kV and 30 mA, respectively. A CuK (l = 1.54) x-ray generator target with a maximum power of 3 kW and a goniometer that can measure 2-theta angles from 0° to 162° were included in the XRD apparatus.

2.2.2. X-ray fluorescence spectrometry

Using the Rigaku ZSX Primus II with SQX analysis software, X-ray fluorescence spectrometry (XRF) analysis was carried out to ascertain the chemical makeup of the sample. 10 g samples were weighed, combined with 2 g of binder, and pelletized under 20 tonnes of pressure to create pellets that were 35 mm in diameter and 2.5 mm thick. After the pellets had been prepared, they were placed in the spectrometer for chemical analysis.

2.2.3. Scanning electron spectroscopy-energy dispersive spectroscopy

A TESCAN: Vega 3X was used for the scanning electron microscope (SEM) examination, with an electron source with a tungsten filament being used. The surface morphology of the material was recorded utilising backscatter and secondary detectors at a high voltage of 20 kV. Vega software was used to capture images at various magnifications. The energy dispersive X-ray spectroscopy (EDS) analysis done using Oxford's INCA software determined the chemical composition of the chosen locations.

2.2.4. Temperature programmed reduction study

Micromeritics Auto Chem II equipment was used to do the temperature programmed reduction (TPR) experiments. A 50 mg mass of the catalyst was placed inside a quartz tubular reactor, with a thermocouple being used to monitor the temperature of the sample continuously. A furnace was used for heating purpose. The calcined catalyst was flushed with high-purity argon at a temperature of 200 °C for 30 min to remove water and any other impurities before the TPR test was done. It was allowed to cool to room temperature, and a 5 % H_2/Ar mixture was then introduced into the chamber, and the temperature increased from 50 to 850 °C at a rate of 10 °C/min. The volume of gas passing through the reactor was controlled by three Brooks mass flow controls. The amount of H_2 used and the thermal conductivity detector (TCD) signal were automatically recorded by a computer.

2.3. Evaluation of FT performance

A fixed-bed micro-reactor with an internal diameter of 1.6 cm and a length of 25 cm was used for the FTS. A gas cylinder containing syngas and a mixture of H_2/CO/N_2 (purity: 99.99; 60/30/10 vol %) was used to feed the reactant gas stream to the FT reactor loaded with the prepared catalyst, using a flow rate of 10 mL/min and pressure of 10 bar(g). To achieve precise mass balance calculations, N_2 was used as an internal standard. Three catalysts weighing 1.0 g with 10 % Co loading were reduced in-situ for 16 h at 350 °C with pure hydrogen (ca. 99.99 %).

After the reduction stage, the temperature of the reactor was reduced to ambient temperature under nitrogen flow and then raised to 220 °C under synthesis gas at a pressure of 10.85 bar (abs). A hot trap was installed immediately after the reactor to collect wax. It was kept at 150 °C. The oil and water mixture were collected in a second trap that was held at room temperature. After the reactor, all the gas lines were kept at 100 °C. A metering valve was used to control the flow, while a bubble meter was used for the flow measurements. Online gas chromatography was used for online analysis of the product stream. A TCD with a Porapak Q packed column (1.50 m long and 3 mm in diameter) was used to evaluate H_2, N_2 and CO. A flame ionization detector (FID) with a Porapak Q packed column was used to analyse the hydrocarbons online.

2.4. FTS calculations

Quantitative analysis was performed on the information that was obtained from the online GC. As an internal reference for measuring the TCD data, the nitrogen (with a 10 vol percent concentration of N_2) present in the syngas feed of the FT tests was used. The initial calculations done consisted of determining the molar flow rate of the reactants and products. Additional calculations were then done. The calculations used to determine the mass balance, including the conversion of the reactant CO are similar to those used by previous researchers, while the experimental method used was developed many years ago.

The online data that was gathered was processed statistically. As the internal benchmark for the measurement of the TCD data, N_2 (10 vol percent of N_2) present in the syngas feed of the FT tests was used. Further calculations were done after the molar flow rates of the reactants and products had been established. The equations used to calculate the mass balance, including the conversion of the reactants CO and H_2 are provided below (see equation (1)).

$$\% CO = \frac{F_{in}X_{CO,in} - F_{out}X_{CO,out}}{F_{in}X_{CO,in}} \quad (1)$$

where: $X_{CO,in}$ denotes the molar fraction of CO in the reactor's gas feed; $X_{CO,out}$ is the molar fraction of CO in the gas stream exiting the reactor.

The CO consumption rate is determined as given by equation (2) given below:

$$r_{CO}=\frac{F_{out}X_{CO,out}-F_{in}X_{CO,in}}{m_{cat}} \tag{2}$$

where: r_{CO} is the rate of CO consumption; mol/(min.g_{cat}), m_{cat} is the mass of the catalyst utilized in this reaction, which is denoted by the variable m cat, and expressed in grams. The rate of gas product generation θ_i , mol/(min.g_{cat}) can be calculated as given in equation (3) below:

$$r_{\theta_i}=\frac{F_{out}X_{\theta_{i,out}}}{m_{cat}} \tag{3}$$

where: $X_{\theta_{i,out}}$ represents the molar fraction of the fraction of θ_i in the gas stream exiting the reactor.

Based on the moles of carbon, the product selectivity was determined using the following calculation (see equation (4)):

$$Sel\ (\theta)=\frac{[nC]_{\theta}}{-r_{CO}.t.m_{cat}} \tag{4}$$

where: the selectivity of the product θ is denoted by the symbol Sel (θ); the number of moles of carbon present in the product is denoted by the symbol $[nC]_{\theta}$..

2.5. Catalyst characterization using DOE

2.5.1. DOE using RSM

The FT data used as input for DOE were extracted from the literature on cobalt-based catalysts. Using the response surface approach, the effects of numerous independent and dependent variables were examined. The formulation variables and their levels are given in Table 1. The dependent variables were selectivity of C_1 (%), C_2–C_4 (%) and C_{5+} (%) following FTS over a cobalt-based catalyst. The three independent variables were crystallite size (a), reaction pressure (b) and reaction temperature (c). A design matrix of the investigated responses is provided in Table 2.

The effect of the independent variable on responses were modelled as per Montgomery (2013) [21], using the second-order polynomial equation involving independent factors and interaction factors. This was pre-selected based on model analysis, lack of fit and R^2 analysis measured responses. To simulate the effect of the independent factors on crystallite size (a), reaction pressure (b) and reaction temperature (c), the following quadratic mathematical model (**equation (5)**) was created using optimization design:

$$f=a_0+\sum_{i=1}^{m}a_iZ_i+\sum_{i=1}^{m}a_{ii}Z_i^2+\sum_{i<j}^{m}a_{ij}Z_iZ_j \tag{5}$$

where: Y is the response; a_0 is the intercept; a_i, a_{ii}, and a_{ij} are regression coefficients; Z_i and Z_j represent individual effects; quadratic effects are represented by Z^2; interaction effects are represented by Z_iZ_j.

The optimization results were evaluated using ANOVA analysis.

Statistical software was used to optimize the design, create the projected FTS product selectivity, and display the effect of the variable parameters on product output, using RSM graphics. The ANOVA data analysis shows the analysis of variance, the significance of the variance test and the first-order coefficient significance test regression equation, all of which were employed to evaluate the reliability of the model.

2.5.2. Descriptive statistics and model fitting

Statistical evaluation of the model included using version 13 of Design Expert for regression analysis of the experimental data to match the equations, while the correlation coefficient (R^2) was used to determine the validity of the resulting model. The significance of the ANOVA equations that were established was also determined using analysis of variance.

3. Results and discussion

The results were used to analyse the operating conditions (temperature, pressure, and cobalt crystallite size), with the end goal

Table 1
DOE reaction parameters and limits.

Factor	Name	Units	Minimum	Maximum
1	Cobalt crystallite size	nm	3.00	26.0
2	Pressure	Bar	5.00	20.0
3	Temperature	°C	200	270

Table 2
Experimental responses and predicted responses obtained by means of RSM.

Data source	Run	Factor 1	Factor 2	Factor 3	Response 1		Response 2		Response 3	
		Crystallite size	Pressure	Temperature	C_1		C_2–C_4		C_{5+}	
		nm	bar	°C	Predicted	Actual	Predicted	Actual	Predicted	Actual
1	1	13.8	20.0	220	19.2	21.3	13.9	15.5	67.9	63.2
	2	17.6	20.0	220	20.5	18.5	13.4	14.8	67.0	66.7
	3	9.50	20.0	220	18.7	14.1	19.9	11.7	62.4	74.2
2	4	5.90	20.0	220	19.2	19.2	29.3	36.6	52.5	44.2
	5	6.80	20.0	220	19.0	20.4	26.6	35.4	55.4	44.2
	6	14.1	20.0	220	19.2	17.9	13.7	19.1	68.1	63.0
3	7	3.00	5.00	250	40.9	40.0	48.3	57.0	11.7	3.00
	8	5.50	5.00	250	35.2	48.0	40.3	34.0	25.4	18.0
	9	8.60	5.00	250	28.7	25.0	33.1	40.0	39.1	35.0
4	10	9.00	10.0	230	17.4	36.4	10.1	3.80	73.5	59.9
	11	13.0	10.0	230	14.4	11.0	5.40	1.80	81.2	87.2
	12	14.3	10.0	230	13.6	11.8	5.00	2.30	82.4	85.9
	13	17.0	10.0	230	12.3	19.3	5.70	3.50	83.0	77.1
5	14	26.0	15.0	200	46.4	44.0	28.6	23.7	26.0	32.3
	15	3.00	15.0	200	22.8	18.7	30.1	20.9	48.0	60.4
	16	6.70	15.0	200	24.4	28.5	18.7	16.7	57.8	54.8
	17	6.90	15.0	200	24.5	19.2	18.2	19.0	58.2	61.8
	18	8.30	15.0	200	25.3	37.6	15.1	18.7	60.5	43.7
6	19	3.00	15.0	220	18.3	12.1	22.9	16.9	59.8	71.0
	20	6.70	15.0	220	16.5	17.5	10.8	13.1	73.7	69.4
	21	6.90	15.0	220	16.4	11.2	10.3	14.8	74.3	74.0
	22	8.30	15.0	220	16.0	13.7	7.00	14.2	78.1	72.1
7	23	6.50	10.0	220	21.3	24.2	19.7	22.4	60.0	53.4
	24	10.0	10.0	220	19.7	16.1	12.9	16.5	68.4	67.4
	25	11.2	10.0	220	19.3	14.4	11.4	15.4	70.3	70.2
	26	7.10	10.0	220	21.0	20.0	18.2	16.2	61.8	63.8
	27	11.0	10.0	220	19.3	17.8	11.6	16.5	70.0	65.7
	28	15.4	10.0	220	18.6	16.1	9.90	11.0	72.5	72.9
8	29	15.0	20.0	270	17.0	17.5	17.2	27.3	65.0	54.3
	30	16.0	20.0	270	15.0	19.0	16.6	11.4	67.6	65.9
	31	16.0	20.0	270	15.0	8.20	16.6	12.6	67.6	78.6
	32	10.0	20.0	270	27.8	35.4	25.1	22.1	46.5	41.7
	33	10.0	20.0	270	27.8	22.2	25.1	30.7	46.5	44.8
9	34	6.20	20.0	220	19.2	28.4	28.4	25.3	53.5	46.3
	35	11.4	20.0	220	18.8	19.5	16.5	15.8	65.7	64.7
	36	13.8	20.0	220	19.2	21.3	13.9	15.5	67.9	63.2
	37	17.6	20.0	220	20.5	18.5	13.4	14.8	67.0	66.7
	38	9.50	20.0	220	18.7	14.1	19.9	11.7	62.4	74.2
	39	5.90	20.0	220	19.2	19.2	29.3	36.6	52.5	44.2
	40	6.80	20.0	220	19.0	20.4	26.6	35.4	55.4	44.2
	41	14.1	20.0	220	19.2	17.9	13.7	19.1	68.1	63.0
10	42	3.00	5.00	250	40.9	40.0	48.3	57.0	11.7	3.00
	43	5.50	5.00	250	35.2	48.0	40.3	34.0	25.4	18.0
	44	8.60	5.00	250	28.7	25.0	33.1	40.0	39.1	35.0
	45	11.0	5.00	250	24.0	5.00	29.6	10.0	47.3	85.0
11	46	11.9	20.0	230	15.9	20.6	14.7	10.7	70.2	68.8
	47	10.8	20.0	230	16.3	13.91	16.5	8.23	68.0	77.66
	48	10.5	20.0	230	16.5	14.94	17.1	9.67	67.3	75.39
	49	10.6	20.0	230	16.4	15.25	16.9	9.67	67.5	75.09
	50	10.4	20.0	230	16.5	17.4	17.3	15.2	67.1	67.42
	51	9.98	20.0	230	16.7	18.47	18.0	16.0	66.1	65.52
12	52	19.7	10.0	240	5.80	10.6	4.50	8.20	90.6	81.2
	53	18.6	10.0	240	6.60	10.7	3.10	8.50	91.2	80.8
	54	18.0	10.0	240	7.10	9.90	2.50	7.50	91.3	82.6
	55	9.20	10.0	240	16.4	15.7	6.40	8.00	78.1	75.8
	56	6.30	10.0	240	20.6	17.9	13.0	10.5	67.4	71.6
	57	4.90	10.0	240	22.7	12.6	17.1	7.80	61.1	79.6

being to identify the optimal operating parameters indicated by the results of the preliminary research. The experimental matrix was used to collect 57 experimental series from 12 different data sources. Table 2 provides the experimental and predicted values for the various experimental settings used that were taken from the published research [22–25]. The actual values for C_1, C_2–C_4 and C_{5+} selectivity acquired by performing actual FTS were compared with the predicted values, with the results showing that they were rather similar. All possible mechanisms of interaction and the reactions of variables were explored using statistical analysis of the results. Prior to determining the statistical significance, the impact of residuals were examined to determine the adequacy of the testing and

optimization performed.

The residual values, which represented the discrepancy between the expected results and the ones obtained from optimization. External studentized residuals were used to evaluate the regression assumptions, with all the different normal distributions mapped onto a single standard normal distribution, which makes it easier to note problems with the analysis. The normal probability plots provided in Fig. 1, Figs. 2 and 3 show whether the residuals followed a normal distribution.

When a sequenced factorial design is used for screening (finding statistically significant factors), high-order interactions can occur [21]. A normal probability plot based on the coefficient of effects was formed to estimate the important effects based on their amounts and calculate their growing probabilities [26]. A normal probability plot depicts the relationship between actual value evaluations and their accumulative normal probabilities [21]. Figs. 1–3, show the normal probability plots with a straight line of best fit, which indicates that the hypothesis is correct and that the models are adequate to produce the desired products. Another indication of the adequacy of the model is a pattern of experimental points being within the limiting constraints of the line of best fit.

A one-way ANOVA test was used to determine the statistical significance in describing selectivity behaviour. The statistical significance of the models used as predictive models is indicated by a p-value of less than 0.05 obtained during the ANOVA for C_1, C_2–C_4 and C_{5+}. Furthermore, a strong correlation between model-predicted and experimental results indicates well-fitted, accurate models.

3.1. Model fitting and analysis of variance

ANOVA was used to analyse the impact of individual factors and their interactions as well as the statistical significance and goodness of fit of the established second-order quadratic models. The results are summarized in Table 3. In statistical analysis, it is imperative for the P-value to fall below the threshold of 0.05 to establish the significance of factors on the response values, as highlighted by Montgomery (2013) [21]. In the context of our study, the analysis of variance (ANOVA) results reveals P-values of 0.001, 0.02, and 0.005 for C_1, C_2–C_4, and C_{5+} factors, respectively. These low P-values strongly indicate the statistical significance of the models at a 95 % confidence level.

Furthermore, it's crucial to note that the magnitude of an independent variable's influence on the response is directly proportional to the F-value attributed to that variable. This underscores the importance of not only achieving statistical significance but also comprehending the relative impact of each variable on the response values, enhancing the depth of analysis.

The individual impact of the three variables is notably significant only in the case of pressure, where it influences the selectivity of C_{5+}. Temperature exhibits effects on both C_1 and C_{5+} selectivity; however, what's particularly noteworthy is that the quadratic effects, denoted as b^2 and c^2, hold significance. This is evident not only from the quadratic terms present in the models for C_1 and C_{5+} but also from the estimated F-values and a P-value of 0.05.

These findings underscore the substantial influence of temperature and pressure on the selectivity of both C_1 and C_{5+}. Additionally, the interactive effects between crystallite size and temperature also emerge as significant contributors to the selectivity of C_1 and C_{5+}.

The significance of the models shown in Table 3 is further supported by the examination of the R^2 and adjusted R^2 values shown in Table 4, which show a small percentage difference. These findings show that the test independent variable was in agreement with the model, since the adjusted R^2 takes into account the different independent variables included in the test; the model and R-squared do not do so, but the percentage difference is small.

3.1.1. Model of selectivity for C_1

Lowering C_1 selectivity and enhancing C_{5+} selectivity is an essential consideration in the FT process [7,19,27]. After fitting the

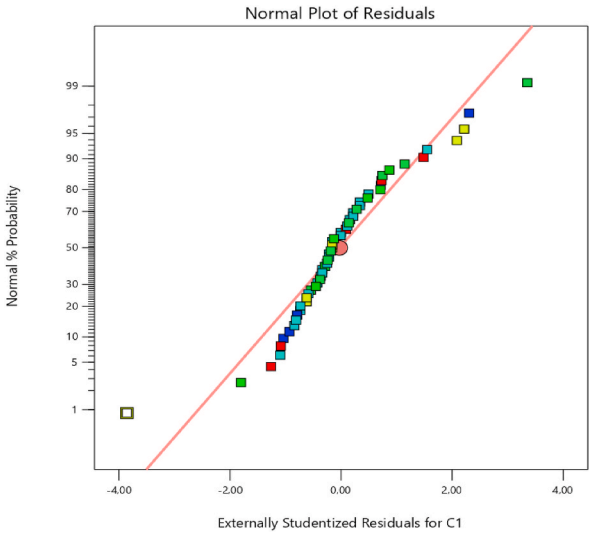

Fig. 1. Normal probability plot of residuals - C_1 selectivity.

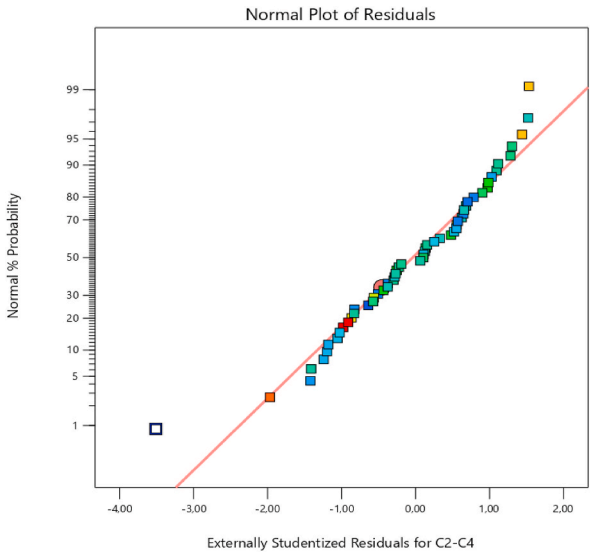

Fig. 2. Normal probability plot of residuals - C_2–C_4 selectivity.

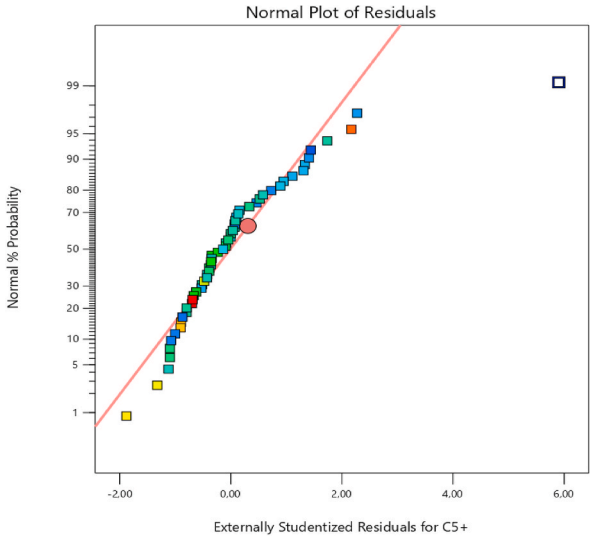

Fig. 3. Normal probability plot of residuals - C_{5+} selectivity.

response data to various models, it was observed that the quadratic model for C_1 selectivity (**equation (6)**) best explained the data. This indicates the effect of the independent variables.

$$S_{C_1} = +538.39143 + 8.87327a - 7.08929b - 4.30395c + 0.0359.5ab - 0.046370ac + 0.030586a^2 + 0.144587b^2 + 0.0009674c^2 \quad (6)$$

where:

a- Crystallite size

b- Reaction pressure

c- Reaction temperature.

C_1 production is presumed to be proportional to crystallite size growth; however, the interaction between crystallite size and temperature shows that increasing crystallite size has a negative influence on C_1 production. (See F**igure 4a and b**.) Saib et al. (2002) [22] reveal another factor that shows a correlation between selectivity and pore diameter: at a low temperature (200 °C) and constant pressure, a reduction in crystallite size is accompanied with a decrease in C_1 selectivity; however, at a high temperature (270 °C), the pattern is the opposite. This phenomenon is depicted in Fig. 4 and supports the ANOVA findings of this study, which indicate that the interaction between crystallite size and temperature is significant. Merino et al. (2016) [28] explain the phenomenon from the perspective of diffusion and the interaction between reactants and active surfaces. As the reaction progresses, wax accumulates and

Table 3
ANOVA for the fitted models of responses.

Model	C_1			C_2–C_4			C_{5+}		
	F-value	p-value		F-value	p-value		F-value	p-value	
Whole-plot	4.86	0.0011	Significant	5.46	0.0235	Significant	9.67	0.0042	Significant
b	0.5628	0.4569		4.83	0.0595		5.96	0.0326	
c	8.19	0.0063		1.67	0.2561		8.99	0.0363	
bc	0.1907	0.6643		0.6588	0.4513		1.59	0.2576	
b^2	2.17	0.1473		10.92	0.016		16.65	0.004	
c^2	9.41	0.0036		1.76	0.2262		9.42	0.0124	
Sub-plot	**7.11**	**0.0001**	**Significant**	**9.23**	**< 0.0001**	**Significant**	**11.5**	**< 0.0001**	**Significant**
a	3.12	0.0836		1.4	0.2426		3.46	0.0695	
ab	0.5449	0.4641		1.09	0.3017		0.0308	0.8614	
ac	12.9	0.0008		0.8317	0.3671		7.8	0.0078	
a^2	0.6006	0.4422		14.48	0.0005		9.52	0.0035	

a- Crystallite size.
b- Reaction pressure.
c- Reaction temperature.

Table 4
Significance of predicted models.

Model	Term df	Error df	F-value	p-value	R^2	Adjusted R^2
C_1	5	47	4.86	0.0011	0.6235	0.5315
C_2–C_4	5	6.92	5.46	0.0235	0.7709	0.7150
C_{5+}	5	7.28	9.67	0.0042	0.7851	0.7326

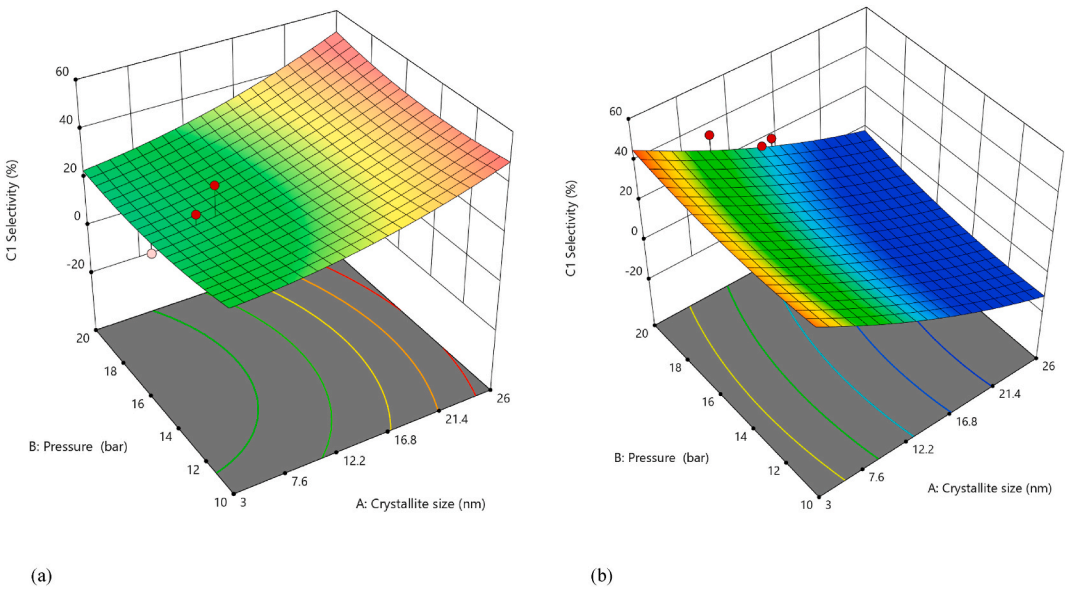

Fig. 4. Effect of temperature on C_1 selectivity at (a) a low temperature - 200 °C; (b) a high temperature - 270 °C.

prevents the reactants from reaching the active site. The activity of Co catalysts during FTS is predominantly determined by the total number of exposed cobalt crystallites. However, CO and H_2 can dissolve and diffuse through the wax to reach the active site [29].

The dissolution and diffusion of reactants into the pore causes a larger hydrogen concentration inside the porous catalyst and an increase in the H_2/CO ratio since H_2 diffuses considerably more rapidly than CO. This supports the chain termination process and affects product selectivity, which frequently results in high C_1 selectivity. Increasing the reaction temperature causes an increase in the reactant dissolution process, particularly CO, which favours chain propagation. Moreover, smaller crystallite size results in more active sites, according to Fang et al. (2020) [30]. When the crystallite size is reduced, the number of exposed cobalt atoms on the support surface increases, making it easier for CoO to form, which results in high C_1 selectivity [30].

An increase in pressure along with an increase in crystallite size resulted in a slight decrease in the production of C_1 molecules at a high temperature of 270 °C. (See Fig. 5 (a and b). A plausible reason before this is that increased pressure in the system forces free-moving molecules to compact together, thus promoting chain propagation. In accordance with Le Chatelier's principle, raising the pressure allows the system to regain equilibrium, which results in a decrease in C_1 and an increase in heavy C_{5+}.

Fig. 5(a and b) shows that at both a high and a low temperature (200–270), and regardless of pressure fluctuation, significantly high levels of C_1 are noticed with: a high temperature and a small crystallite size; a low temperature and a large crystallite size. Minimal C_1 generation is noted with a high temperature (270 °C) and a large crystallite size (26 nm). This shows that temperature influenced either conversion to light hydrocarbons or conversion to heavy hydrocarbons.

3.1.2. Model of selectivity for C_2–C_4

The proportion of low-weight hydrocarbon is expressed as a percentage of C_2–C_4 and has little correlation with individual variables. Crystallite size and pressure affect C_2–C_4 production quadratically on an individual basis. The temperature has a negative impact on C_2–C_4 production. Experimental data analysed using ANOVA showed that: the quadratic effect of crystallite size and pressure had a significant impact on C_2–C_4 generation; the quadratic model had lower R^2 values due to the lack of a fit test and model summary statistics.

The quadratic model was used to investigate the effect of independent factors on C_2–C_4 production, Equation (7) shows the mathematical equation in terms of factors:

$$S_{C_2-C_4} = +551.70634 + 2.02503a - 21.32657b - 3.08382c + 0.051173ab - 0.008965ac + 0.035672bc + 0.155881a^2 + 0.486340b^2 + 0.005274c^2 \quad (7)$$

where:

a- Crystallite size

b- Reaction pressure

c- Reaction temperature.

Even though only the quadratic effect of crystallite size and pressure are significant, the sub-plot ($p < 0.0001$) and the whole plot ($p < 0.05$) are statistically significant, according to the ANOVA results. Crystallite size has a significant quadratic effect on C_2–C_4 formation.

Fig. 6(a and b) illustrates the adverse impact of temperature when the interactions of temperature and crystallite size are taken into consideration. As the temperature rises, the generation of $C_2 - C_4$ decreases, which demonstrates how temperature can have a negative impact, therefore appropriate conditions need to be selected. In addition, the interaction between crystallite size and temperature exhibited a negative coefficient, which suggests a relationship to the response that is inversely proportional.

Fig. 7(a and b) shows that an increase in chain propagation of the C_2–C_4 molecules begins to take place when the pressure is increased. Exactly the same behaviour can be seen in case of Qiu et al. (2017) [31]. During the FT process, cobalt crystallites of a consistently small size adsorb reactants into a confined matrix with high efficiency, which lowers the likelihood of cobalt crystallite clustering and intermediate desorption significantly [31]. This, in turn, results in favourable selectivity for heavier hydrocarbons (see Fig. 8).

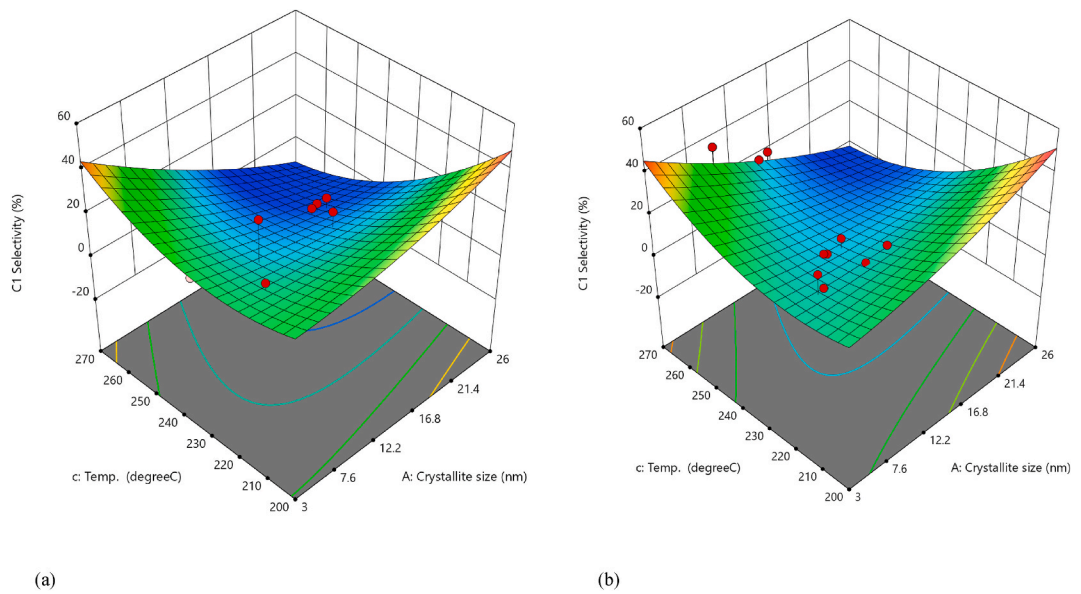

(a) (b)

Fig. 5. Effect of pressure on C_1 selectivity at: (a) a low pressure - 5 bar (g); (b) a high pressure - 20 bar (g).

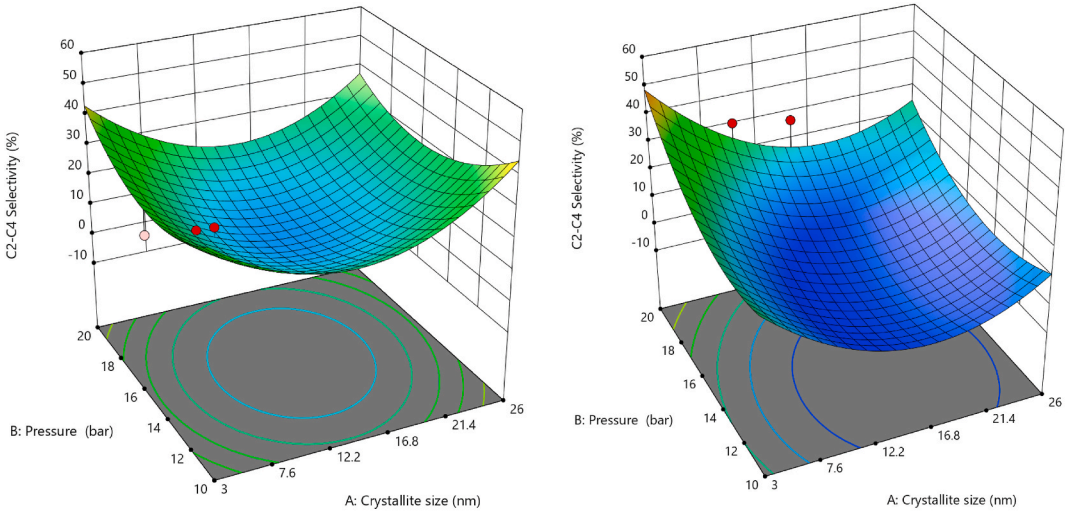

Fig. 6. Effect of temperature on C_2–C_4 selectivity at: (a) a low-temperature - 200 °C; (b) a high-temperature - 270 °C.

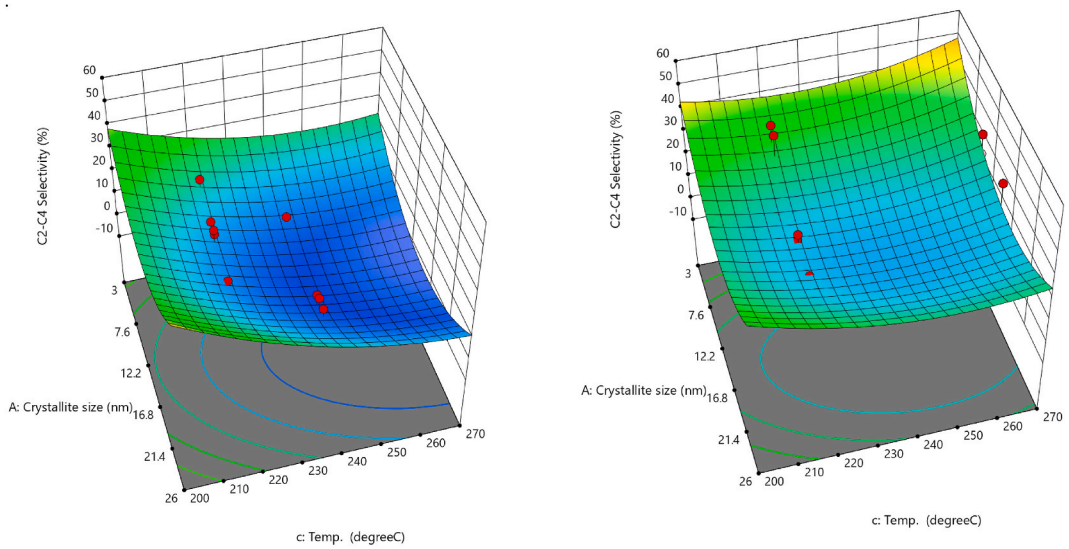

Fig. 7. Effect of pressure on C_2–C_4 selectivity at: (a) a low pressure - 5 bar_g; (b) a high pressure - 20 bar_g.

It is expected that an increase in pressure would cause the balance to move toward the generation of more viscous products and more C_{5+} products. As less viscous wax favours chain propagation, the subsequent dissolution of CO and H_2 would serve as a wax plasticizer, resulting in an increase in heavy hydrocarbons.

The effect of both temperature and pressure show that the desired product generation (C_2–C_4) is achieved at size extremes of crystallite - whether small or large. To produce more C_2–C_4, optimal operation is required at a low pressure (5 bar_g) and a low temperature (200 °C), as the crystallite effect will not be significant. A high temperature is required (270 °C) at a high pressure (20 bar_g), regardless of the size of the crystallite. The study done by Wang et al. (2012) [32] yielded the required products when the cobalt crystallite measured an average 9.9 nm, which corresponds to the same range observed on the RSM diagrams in this study. The equilibrium of C_2–C_4 seems to shift as the size of the crystallite is moved from extreme large to extremely low. The three groups of products (C_1, C_2–C_4 and C_{5+}) tend to behave antagonistically, depending on the parameters employed.

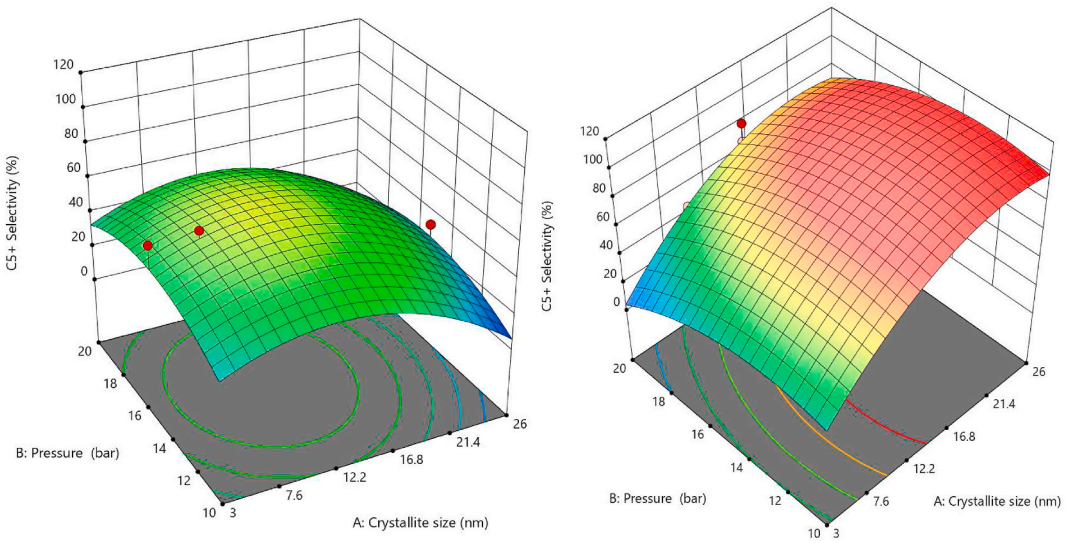

Fig. 8. Effect of temperature on C_{5+} selectivity at: (a) a low temperature - 200 °C; (b) a high temperature - 270 °C.

3.1.3. Model of selectivity for C_{5+}

To thoroughly examine the impact of independent factors, including crystallite size, pressure, and temperature, on the production of C_{5+}, a quadratic model was used. This modelling approach enabled a detailed exploration of how variables interact and affect the desired output.

The identification of significant model terms was a critical step in the analysis. Among these terms, the factors b, c, ac, a^2, b^2, and c^2 stood out as highly influential in shaping the production outcomes. Their presence within the model indicates that changes in these factors have a considerable impact on the production of C_{5+}. In contrast, model terms with P-values exceeding 0.1000 were considered non-essential and therefore excluded from our focused examination.

To validate the significance of these selected terms, an analysis of variance (ANOVA) with a sub-plot and whole-plot approach was used. The low p-value obtained in the sub-plot analysis ($p < 0.0001$) and the still significant p-value in the whole-plot analysis ($p < 0.05$) further confirmed the statistical significance of these factors.

Considering the individual contributions of these factors, it is evident that both pressure and temperature are substantial and vital variables in the production process. Each factor plays a unique and indispensable role in influencing the production of various products, and their significance is underscored by their strong statistical standing. Their collective influence serves as a cornerstone in shaping the overall production dynamics and is an essential element of this comprehensive analysis.

Equation (8) illustrates the mathematical equation in terms of factors:

Model of selectivity for C_{5+}:

$$S_{C_{5+}} = -1015.54237 - 6.70152a + 28.95110b + 7.58213c + 0.014172ab + 0.054825ac - 0.048173bc - 0.187267a^2 + 0.633187b^2 - 0.015316c^2 \quad (8)$$

where:

a- Crystallite size (nm).

b- Reaction pressure (bar).

c- Reaction temperature (°C).

According to the experimental results, C_{5+} selectivity showed an unusual increase with an increase in temperature. In general, FTS results in heavy products at a low temperature with a high straight-chain paraffin content. A high temperature result in lighter products with a higher straight-chain paraffin content, as well as secondary reactions like chain cessation and short-term chain termination. A low temperature increases the wax yield considerably, while reducing light gas output.

When the reaction temperature and crystallite content were increased, the rate of C_{5+} generation increased in an exponential fashion. However, a linear rise in both crystallite content and temperature resulted in an increase in C_{5+} selectivity. Increasing the temperature when there was a low crystallite content resulted in a decrease in the amount of C_{5+} produced (See Fig. 1.8 a and b.). Qiu et al. (2017) [31] attributed this to controlled particle size.

Selectivity for C_1 increased with reaction temperature at low crystallite sizes, whereas for C_{5+} increasing temperature enhances productivity with a larger crystallite size. When Qiu et al. (2017) [31] and Liu et al. (2017) [33] findings were compared, small crystallite sizes led to reduced CO hydrogenation activity and enhanced C_1 selectivity, whereas a larger crystallite size favoured C_{5+}

products. The most likely rationale is related to fluid properties, specifically the rheological properties of wax in terms of reactant dissolution prior to reaching the reaction surface. With less viscous fluid properties, as a result of temperature change, more CO and H_2 diffuse through the wax, which reduces the chances of chain termination due to hydrogen influx near the active site. This resulted in the chain extension. When increasing the particle size, the catalytic activity increased, while the structural properties remained unchanged. Selectivity to C_{5+} decreased as particle size decreased at 270 °C. This is consistent with the findings of Wang et al. (2012), who revealed that increasing the size of the cobalt particle improves the turnover frequency for CO conversion, which could be due to increased CO site coverage [32]. This then increases C_{5+} selectivity. Saib et al. (2002) shared the same results [22].

The viscosity of the reaction tends to rise when pressure is applied. It is hypothesised that the effect is caused by the convective free volume, which decreases when pressure is applied. This causes an increase in internal air resistance, which raises viscosity and C_{5+} selectivity. The increase in viscosity is dependent on the specific C_{5+} compound. However, the effect of pressure is much smaller than the effect of temperature. The fluids in the process exhibit a minimal viscosity shift at moderate pressure, so the effect of pressure is frequently overlooked. Increased pressure has a greater impact on heavier C_{5+} hydrocarbons, which suggests that pressure has a greater impact on C_{5+} products than on C_1 and C_2–C_4 Products. The pressure effect can be enhanced by branched waxes, which have more free intrinsic volume. As illustrated in Fig. 9, as pressure increases, so C_{5+} selectivity increases.

3.2. Determining optimum conditions

An experiment was carried out with the parameters that were recommended by the model to determine whether the optimum conditions that were provided by the model were reliable. The conditions proposed for use in the confirmatory experiment were as follows: crystallite size = 11 nm; pressure = 10 Bar_g; temperature = 220 °C. Fig. 10 illustrates the optimum conditions.

Of the catalysts manufactured with varying particle sizes for the support, the three with the most similar crystallite size were used, i.e.: 75 to +53 μm; −53 to +38 μm; less than 25 μm. Run 1 represents particles with a catalyize class of −75 to +53 μm. Run 2 represents the support size class −53 to +38 μm, and run 3 the support particle size class of less than 25 μm. The results shown are the average of the runs carried out using the same experimental conditions. During optimization, the required set parameters were set to prioritize higher C_{5+} generation. As shown in Table 5, the model can be considered to fit the experimental data under these experimental conditions. It was demonstrated that the optimum conditions for achieving the required high C_{5+} are large crystallites (11 nm), a low temperature (220 °C) and a somewhat high pressure (10 bar_g). Furthermore, the optimization process and test runs prove that the experimental design is replicable and reliable enough for use in predicting end products.

The outcomes of three FTS tests are provided in Table 5. An examination and comparison of these findings to the model's optimal values, leads to the conclusion that the results are reliable and that they can be replicated. Therefore, the factors that were selected were validated as being appropriate.

4. Conclusion

The study of optimizing product selectivity within the context of this study has resulted in valuable information on process parameters and how they affect FTS. This has not only allowed gaining deeper insights into the design of our experiments but has also

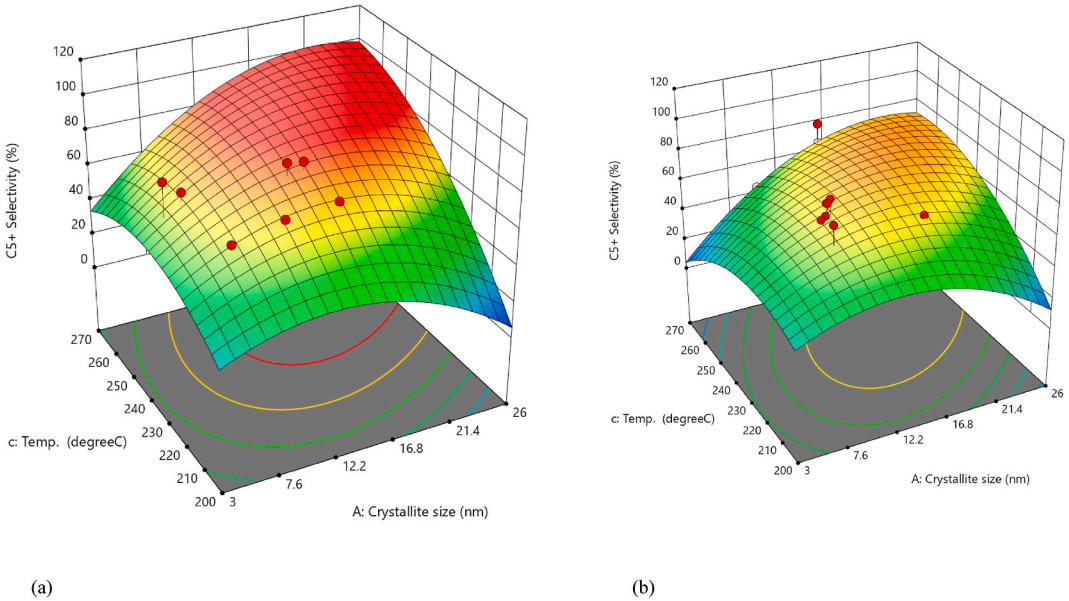

Fig. 9. Effect of pressure on C_{5+} selectivity at: (a) low-pressure; (b) a high-pressure.

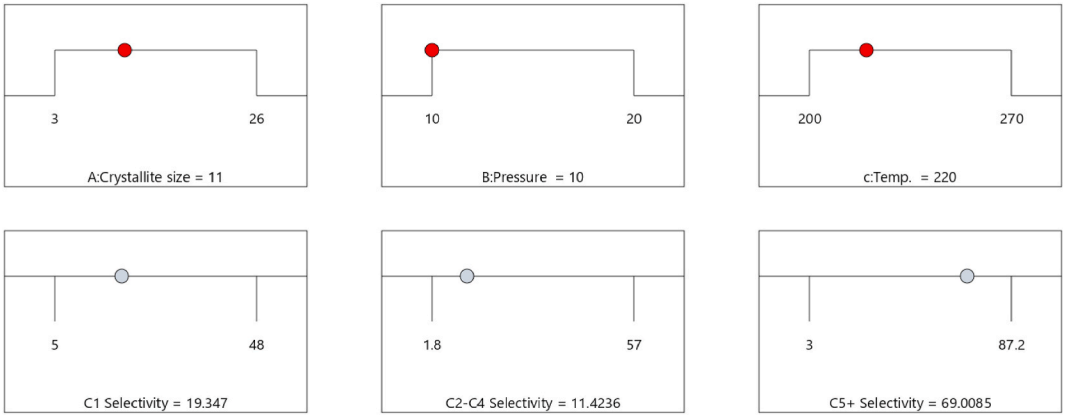

Fig. 10. Optimized design parameters for the proposed FT process.

Table 5
Product generation at optimal conditions.

Data Source	Run	Factor 1	Factor 2	Factor 3	Response 1		Response 2		Response 3	
		Crystallite size	Pressure	Temperature	C_1		C_2–C_4		C_{5+}	
		nm	bar	°C	Predicted	Actual	Predicted	Actual	Predicted	Actual
Experiment	**1**	9.24	10.0	220	19.96	19.79	13.60	14.17	65.99	66.08
	2	9.22	10.0	220	19.97	19.79	13.62	14.19	65.95	66.05
	3	8.27	10.0	220	20.84	20.12	15.17	15.72	63.84	64.21
Model		**11**	**10.0**	**220**	**19.35**	**19.38**	**11.42**	**11.77**	**69.01**	**68.99**

revealed the potential for modifying designs to precisely obtain the desired products. The primary goal of the Design of Experiments (DOE) was to optimize the efficiency of the cobalt-based Fischer-Tropsch (FT) catalyst and ensure that the product groups remained within the specified range.

Key factors that significantly influence the composition of the final product include crystallite size, reaction temperature, and pressure during the FT reaction. A comprehensive investigation of product distribution and yield, expressed as proportions of total hydrocarbons, using Response Surface Methodology (RSM) and estimated distribution models was used. This in-depth analysis allowed identification of how system parameters and model parameters directly influence the projected product distribution, emphasizing the strong connection between operating conditions and the final product mix.

The statistical significance of the parameters under investigation became evident after examining the findings through probability distributions. By adjusting the operating settings, it was observed that there is a possibility of shifts in product selectivity. Altering these parameters also corresponded to variations in the average number of carbon atoms within the hydrocarbon derivatives. Among these parameters, cobalt crystallite size, reaction temperature, and pressure emerged as statistically significant factors that exerted a substantial impact on the formation of C_1, C_2–C_4, and C_{5+} products. However, it's worth noting that pressure was found to be statistically inconsequential, holding no significant influence over the formation of these product groups.

With the identification of these significant factors, optimization of parameters using Response Surface Methodology (RSM) was performed. Through this optimization, it was pinpointed the most favourable conditions: a crystallite size of 11 nm, a pressure of 10 Bar, and a temperature of 220 °C. Subsequent confirmatory tests, which closely mirrored these settings, further validated the selection of these optimum conditions. Preference was to get maximum C_{5+} output.

In summary, these conclusions from results were drawn.

1. The methodological approach and experimental design employed proved effective in discerning both statistically significant and insignificant components under investigation.
2. The high R^2 values indicate that the model developed can provide reasonably accurate response estimates for the system within the study's scope.
3. The statistical analysis, especially evident in the normal probability plot, vividly demonstrated the significant influence of the parameters and their respective distributions.
4. The model's compatibility with the experimental data under these specific conditions opens the possibility of adapting it to light hydrocarbons, an area not explored in this study but encountered during the process. This adaptability suggests the model's potential for broader applications.

In essence, this study has not only yielded significant insights into the optimization of product selectivity but also unveiled the

potential for broader adaptability and applications of the methodologies employed.

Data availability

Data will be made available on request.

CRediT authorship contribution statement

Roick Chikati: Writing - original draft, Project administration, Methodology, Investigation, Data curation, Conceptualization. **Tawanda A. Mpandanyama:** Writing - original draft, Writing - review & editing, Validation, Methodology, Investigation, Formal analysis, Data curation, Conceptualization. **Diankanua Nkazi:** Writing - review & editing, Validation, Supervision, Resources, Project administration, Methodology, Funding acquisition. **Phathutshedzo Khangale:** Writing - review & editing, Validation, Resources, Methodology, Data curation, Conceptualization. **Joshua Gorimbo:** Writing - review & editing, Validation, Supervision, Methodology, Formal analysis, Data curation, Conceptualization.

Declaration of competing interest

The authors declare that they have no known competing financial interests or personal relationships that could have appeared to influence the work reported in this paper.

References

[1] Y. Wang, Y. Tian, S.Y. Pan, S.W. Snyder, Catalytic processes to accelerate decarbonization in a net-zero carbon world, ChemSusChem 15 (24) (2022), https://doi.org/10.1002/cssc.202201290.
[2] J. Gorimbo, An Experimental and Thermodynamic Study of Iron Catalyst Activation and Deactivation during Fischer Tropsch Synthesis, University of the Witwatersrand, 2016.
[3] A.Y. Khodakov, Fischer-Tropsch synthesis: relations between structure of cobalt catalysts and their catalytic performance, Catal. Today 144 (3–4) (2009) 251–257, https://doi.org/10.1016/j.cattod.2008.10.036.
[4] M.E. Dry, The fischer - tropsch process: 1950-2000, Catal. Today 71 (2002) 227–241, https://doi.org/10.1016/S0920-5861(01)00453-9, 3–4.
[5] M.J.A. Tijmensen, A.P.C. Faaij, C.N. Hamelinck, M.R.M. Van Hardeveld, Exploration of the possibilities for production of Fischer Tropsch liquids and power via biomass gasification, Biomass Bioenergy 23 (2) (2002) 129–152, https://doi.org/10.1016/S0961-9534(02)00037-5.
[6] J. Gorimbo, X. Lu, X. Liu, D. Hildebrandt, D. Glasser, A long term study of the gas phase of low pressure Fischer-Tropsch products when reducing an iron catalyst with three different reducing gases, Appl. Catal. Gen. 534 (2017), https://doi.org/10.1016/j.apcata.2017.01.013.
[7] J. Yang, W. Ma, D. Chen, A. Holmen, B.H. Davis, Fischer-Tropsch synthesis: a review of the effect of CO conversion on methane selectivity, Appl. Catal. Gen. 470 (2014) 250–260, https://doi.org/10.1016/j.apcata.2013.10.061.
[8] E. Rytter, Ø. Borg, N.E. Tsakoumis, A. Holmen, Water as key to activity and selectivity in Co Fischer-Tropsch synthesis: Γ-alumina based structure-performance relationships, J. Catal. 365 (2018) 334–343, https://doi.org/10.1016/j.jcat.2018.07.003.
[9] E. Makhura, J. Rakereng, O. Rapoo, G. Danha, Effect of the operation parameters on the Fischer Tropsch synthesis process using different reactors, Procedia Manuf. 35 (2019) 349–355, https://doi.org/10.1016/j.promfg.2019.05.051.
[10] S.H. Kang, J.W. Bae, P.S.S. Prasad, K.W. Jun, Fischer-Tropsch synthesis using zeolite-supported iron catalysts for the production of light hydrocarbons, Catal. Lett. 125 (3–4) (2008) 264–270, https://doi.org/10.1007/s10562-008-9586-2.
[11] A.Y. Khodakov, W. Chu, P. Fongarland, Advances in the development of novel cobalt fischer-tropsch.pdf, Chem. Rev. 107 (2007) 1692–1744.
[12] E. Van Steen, M. Claeys, K.P. Möller, D. Nabaho, "Applied Catalysis A , General Comparing a cobalt-based catalyst with iron-based catalysts for the Fischer-Tropsch XTL-process operating at high conversion," 549 (2018) 51–59. July 2017.
[13] Q. Cheng, et al., Confined small-sized cobalt catalysts stimulate carbon-chain growth reversely by modifying ASF law of Fischer–Tropsch synthesis, Nat. Commun. 9 (1) (2018) 1–9, https://doi.org/10.1038/s41467-018-05755-8.
[14] Y. Li, J. Yu, Emerging applications of zeolites in catalysis, separation and host–guest assembly, Nat. Rev. Mater. 6 (12) (2021) 1156–1174, https://doi.org/10.1038/s41578-021-00347-3.
[15] J. Gorimbo, A. Muleja, X. Liu, D. Hildebrandt, Fischer – tropsch synthesis : product distribution , operating conditions , iron catalyst deactivation and catalyst speciation, Int. J. Ind. Chem. 9 (4) (2018) 317–333, https://doi.org/10.1007/s40090-018-0161-4.
[16] W. D. Shafer et al., "Fischer – Tropsch : Product Selectivity – the Fingerprint of Synthetic Fuels,".doi: 10.3390/catal9030259..
[17] J. Gorimbo, X. Lu, X. Liu, Y. Yao, D. Hildebrandt, D. Glasser, Low-pressure fischer-tropsch synthesis: in situ oxidative regeneration of iron catalysts, Ind. Eng. Chem. Res. 56 (15) (2017), https://doi.org/10.1021/acs.iecr.7b00008.
[18] E. Rytter, A. Holmen, Deactivation and regeneration of commercial type fischer-tropsch Co-Catalysts—a mini-review, Catalysts 5 (2) (2015) 478–499, https://doi.org/10.3390/catal5020478. Mar.
[19] F.E.M. Farias, F.A.N. Fernandes, F.G. Sales, Effect of operating conditions on fischer-tropsch liquid products produced by unpromoted and potassium-promoted iron catalyst, Lat. Am. Appl. Res. 40 (2) (2010) 161–166.
[20] T. Erbach, L. Fan, B. Coulter, S. Kraber, How Experimental Design Optimizes Assay Automation (2004) 1–8, 2004.
[21] D.C. Montgomery, Design and Analysis of Experiments, eighth ed., Arizona State University, 2013, 2009.
[22] A.M. Saib, M. Claeys, E. Van Steen, Silica supported cobalt Fischer-Tropsch catalysts: effect of pore diameter of support, Catal. Today 71 (3–4) (2002) 395–402, https://doi.org/10.1016/S0920-5861(01)00466-7.
[23] D. Song, J. Li, Effect of catalyst pore size on the catalytic performance of silica supported cobalt Fischer-Tropsch catalysts, J. Mol. Catal. Chem. 247 (1–2) (2006) 206–212, https://doi.org/10.1016/j.molcata.2005.11.021.
[24] E. Lira, et al., HMS mesoporous silica as cobalt support for the Fischer-Tropsch Synthesis: pretreatment, cobalt loading and particle size effects, J. Mol. Catal. Chem. 281 (1–2) (2008) 146–153, https://doi.org/10.1016/j.molcata.2007.11.014.
[25] T. Witoon, M. Chareonpanich, J. Limtrakul, Effect of hierarchical meso-macroporous silica supports on Fischer-Tropsch synthesis using cobalt catalyst, Fuel Process. Technol. 92 (8) (2011) 1498–1505, https://doi.org/10.1016/j.fuproc.2011.03.011.
[26] A.S.S. Shapiro, M.B. Wilk, Biometrika, "Biometrika Trust An Analysis of Variance Test for Normality (Complete Samples) Published by : Oxford University Press on behalf of Biometrika Trust Stable," 52 (3) (1965) 591–611 [Online]. Available: https://pdfs.semanticscholar.org/1f1d/9a7151d52c2e26d35690dbc7ae8098beee22.pdf.
[27] J. Gorimbo, G. Charis, Y. Zhang, Y. Richardson, G. Danha, Chapter 15 future aspects of BTL-FTS processes, in: Chemicals and Fuels from Biomass via Fischer–Tropsch Synthesis: A Route to Sustainability, The Royal Society of Chemistry, 2023, pp. 428–456.

[28] D. Merino, I. Pérez-Miqueo, O. Sanz, M. Montes, On the way to a more open porous network of a Co-Re/Al2O3 catalyst for fischer-tropsch synthesis: pore size and particle size effects on its performance, Top. Catal. 59 (2–4) (2016) 207–218, https://doi.org/10.1007/s11244-015-0436-3.
[29] S.H. Huang, H.M. Lin, K.C. Chao, F.N. Tsai, Solubility of synthesis gases in heavy N-paraffins and fischer-tropsch wax, Ind. Eng. Chem. Res. 27 (1) (1988) 162–169, https://doi.org/10.1021/ie00073a030.
[30] X. Fang, et al., Particle-size-dependent methane selectivity evolution in cobalt-based fischer-tropsch synthesis, ACS Catal. 10 (4) (2020) 2799–2816, https://doi.org/10.1021/acscatal.9b05371.
[31] T. Qiu, et al., SAPO-34 zeolite encapsulated Fe3C nanoparticles as highly selective Fischer-Tropsch catalysts for the production of light olefins, Fuel 203 (2017) 811–816, https://doi.org/10.1016/j.fuel.2017.05.043.
[32] Z.J. Wang, S. Skiles, F. Yang, Z. Yan, D.W. Goodman, Particle size effects in Fischer-Tropsch synthesis by cobalt, Catal. Today 181 (1) (2012) 75–81, https://doi.org/10.1016/j.cattod.2011.06.021.
[33] J. Liu, P. Wang, W. Xu, E.J.M. Hensen, Particle Size and Crystal Phase Effects in Fischer-Tropsch Catalysts, vol. 3, 2017, pp. 467–476.